8-15-2012

What can computed tomography and magnetic resonance imaging tell us about ventilation?

Brett A Simon

David W Kaczka

Alexander A Bankier

Grace Parraga

J Appl Physiol 113: 647–657, 2012.
First published May 31, 2012; doi:10.1152/japplphysiol.00353.2012.

HIGHLIGHTED TOPIC | *Imaging Lung Physiology*

What can computed tomography and magnetic resonance imaging tell us about ventilation?

Brett A. Simon,[1,2] David W. Kaczka,[1,2] Alexander A. Bankier,[3,4] and Grace Parraga[5,6,7]

[1]*Department of Anesthesia, Critical Care and Pain Medicine, Beth Israel Deaconess Medical Center, Boston, Massachusetts;* [2]*Department of Anaesthesia, Harvard Medical School, Boston, Massachusetts;* [3]*Department of Radiology, Beth Israel Deaconess Medical Center, Boston, Massachusetts;* [4]*Department of Radiology, Harvard Medical School, Boston, Massachusetts;* [5]*Imaging Research Laboratories, Robarts Research Institute, London, Ontario, Canada;* [6]*Department of Medical Biophysics, The University of Western Ontario, London, Ontario, Canada; and* [7]*Graduate Program in Biomedical Engineering, The University of Western Ontario, London, Ontario, Canada*

Submitted 16 March 2012; accepted in final form 24 May 2012

Simon BA, Kaczka DW, Bankier AA, Parraga G. What can computed tomography and magnetic resonance imaging tell us about ventilation?. *J Appl Physiol* 113: 647–657, 2012. First published May 31, 2012; doi:10.1152/japplphysiol.00353.2012.—This review provides a summary of pulmonary functional imaging approaches for determining pulmonary ventilation, with a specific focus on multi-detector x-ray computed tomography and magnetic resonance imaging (MRI). We provide the important functional definitions of pulmonary ventilation typically used in medicine and physiology and discuss the fact that some of the imaging literature describes gas distribution abnormalities in pulmonary disease that may or may not be related to the physiological definition or clinical interpretation of ventilation. We also review the current state-of-the-field in terms of the key physiological questions yet unanswered related to ventilation and gas distribution in lung disease. Current and emerging imaging research methods are described, including their strengths and the challenges that remain to translate these methods to more wide-spread research and clinical use. We also examine how computed tomography and MRI might be used in the future to gain more insight into gas distribution and ventilation abnormalities in pulmonary disease.

pulmonary physiology; lung imaging; ventilation; gas distribution; ventilation defects

OVERVIEW AND INTRODUCTION

Numerous questions in physiology and medicine have derived solutions or answers from an improved understanding of regional anatomic and functional abnormalities that were qualitatively described or quantitatively measured using medical imaging. For example, over the past four decades, improvements in cardiovascular imaging (9, 63) have paved the way for new regional imaging techniques that have resulted in targeted treatments (17) and vastly improved patient outcomes (30). Clinical applications of anatomic, morphologic, and functional pulmonary imaging have also resulted in improved diagnosis and monitoring in thoracic oncology, as well as in non-neoplastic focal and diffuse lung diseases. There have also been substantial advancements in regional imaging of pulmonary mechanics, as well as ventilation and perfusion in obstructive lung disease, although many of these research tools have not yet been translated to routine clinical use. In particular for clinical applications, static anatomic imaging has dominated, although current research in functional imaging demonstrates great potential for these tools to enhance our understanding of structure-functional relationships in the lung. In this regard, we view quantitative pulmonary functional imaging methods as innovative technologies that provide new ways to answer open clinical questions. Advances in imaging over the last decade provide the physiologist with new tools to investigate lung disease as a regionally heterogeneous system.

Driving the development of regional and quantitative lung imaging techniques are many unanswered questions in pulmonary physiology, along with the growing economic and societal burdens of lung disease with limited therapeutic options. Simultaneously, the trend toward individualized diagnosis and treatment requires sophisticated tools to phenotype diseases and to monitor the effectiveness of treatment. In this regard, pulmonary structure-function imaging tools may provide metrics and answers to unsolved pulmonary problems. In this paper, we discuss the potential for computed tomography (CT) and magnetic resonance imaging (MRI) to provide quantitative insight into pulmonary ventilation. Our main focus is ventila-

Address for reprint requests and other correspondence: G. Parraga, Imaging Research Laboratories, Robarts Research Institute, 100 Perth Dr., London, ON, Canada N6A 5K8 (e-mail: gparraga@robarts.ca).

tion, as it is the primary function of the respiratory system. We also provide critical definitions and examples in an effort to reconcile the occasional divergent viewpoints of the physiologist and imaging scientist. We then summarize recent imaging research in that context. Underscoring and driving the development of all pulmonary imaging approaches is the understanding that global measurements such as those provided by spirometry are insensitive to early disease and that the regional sensitivity of imaging measurements can be exploited to identify ventilation or gas distribution abnormalities that cannot be detected by spirometry.

As several excellent reviews of single photon and positron emission tomography (SPECT and PET) are now available (12, 24, 34, 60), we will mainly focus on functional x-ray CT and MRI and contrast these techniques with other imaging approaches.

DEFINITIONS

An essential function of the respiratory system is the delivery of fresh gas, including oxygen, from the environment to the alveoli and the removal of CO_2 from the body to the external environment. Pulmonary physiology provides clear definitions for this function and derives the term *total pulmonary ventilation* or minute volume ($\dot{V}_E$) as the volume of gas entering the lung per unit time:

$$\dot{V}_E = V_T f \quad (1)$$

where total ventilation $\dot{V}_E$ (in units of ml/min) is simply the tidal volume (V_T) delivered times the breathing frequency per minute (f). Some of the entering tidal volume fills the conducting airways, and thus never reaches the alveoli or participates in gas exchange. Subtracting this ventilation of the anatomic dead space (V_d) defines alveolar ventilation ($\dot{V}_A$):

$$\dot{V}_A = (V_T - V_d) f \quad (2)$$

It is assumed that $\dot{V}_A$ is defined by the delivery of fresh gas (i.e., gas that does not contain CO_2) to the alveoli. Similarly at end expiration, the gas residing in the dead space has the same composition as alveolar gas, and the subsequent reentry of dead space gas to the alveoli does not constitute fresh gas delivery and thus cannot contribute to CO_2 removal. $\dot{V}_A$ can alternately be defined in terms of the ratio of steady state CO_2 production and the alveolar $P_{A_{CO_2}}$, emphasizing the primacy of CO_2 removal in alveolar ventilation:

$$\dot{V}_A = K\frac{\dot{V}_{CO_2}}{P_{A_{CO_2}}} \approx K\frac{\dot{V}_{CO_2}}{P_{a_{CO_2}}} \quad (3)$$

where K is a constant converting the partial pressure of CO_2 to volume (68). Note that under ordinary circumstances, the more easily measured arterial Pa_{CO_2} is very close to the alveolar $P_{A_{CO_2}}$ and can be used to estimate alveolar ventilation in normal lungs. Thus to a physiologist, alveolar ventilation is a steady-state process by which CO_2 is removed from the lung. Gas transport, even of fresh gas, to an alveolar region that is not perfused (and thus does not contain CO_2) does not therefore contribute to alveolar ventilation or gas exchange but rather to dead space ventilation. Particularly in the diseased lung, the delineation of the dead space from gas exchanging regions is not distinct, and the term physiological dead space is used to designate the volume of the lung that functionally does not contribute to CO_2 removal.

Although these relationships are usually described for the entire lung, they also hold true at the regional level, with local alveolar $P_{A_{CO_2}}$ related to the balance of local CO_2 delivery to those alveoli via regional perfusion and the local rate of CO_2 removal via regional ventilation. Note that this is a particularly restrictive definition of alveolar ventilation with respect to effecting respiratory gas exchange; in a broader, more mechanical sense alveolar ventilation could be defined as the delivery of fresh gas to the alveolar zone, independent of CO_2 presence. Most imaging techniques for measuring regional ventilation in fact depend on quantifying the rate of accumulation and/or elimination of a nonabsorbed, inhaled tracer gas in the lung periphery. This approach differs from traditional compartmental modeling of alveolar ventilation and CO_2 removal and thus cannot distinguish alveolar from dead space ventilation. If the tracer gas is either taken up by the pulmonary circulation or delivered to the alveoli from the circulation, similar to the path of the respiratory gases, then it *is* possible to separate dead space from alveolar ventilation as well as estimate ventilation:perfusion ($\dot{V}/\dot{Q}$) ratios, either on a whole lung basis, as with the multiple inert gas elimination technique (62), or regionally, with imaging approaches (34, 43). Thus we urge investigators imaging ventilation to consider whether the distinction between gas transport within the lung and gas exchange with the circulation is important in interpreting their results.

Specific ventilation ($s\dot{V}_r$) is defined as the regional alveolar ventilation normalized by the regional gas volume (V_r), usually at end expiration:

$$s\dot{V}_r = \dot{V}_{A,r}/V_r \quad (4)$$

This parameter arises directly from indicator-dilution techniques that assume an exponential rise of a tracer gas (41). Because ventilation is normalized to a region's gas volume, specific ventilation is a convenient parameter to compare ventilation in different arbitrarily defined pulmonary regions of interest (ROI), because absolute ventilation will increase with the region size.

A similar parameter introduced in the MR literature is the fractional ventilation per breath r, defined as $r = V_f/(V_f+V_o)$, where V_f is the volume of fresh gas entering a region during a breath and V_o the volume of old gas still present in the region at the end of the breath, including the dead space gas (21). Whereas $s\dot{V}_r$ describes the fresh gas entering a lung region (per unit time) normalized to the region's volume at the time of imaging (end-expiratory, mean lung volume, or end-inspiratory), the fractional ventilation r describes the fresh gas (per breath) entering a region normalized to end-inspiratory volume. Thus, if $s\dot{V}_r$ is normalized to regional end-inspiratory volume, r and $s\dot{V}_r$ are equivalent; if $s\dot{V}_r$ is normalized to end-expiratory volume then they are related by $1/r = 1 + 1/s\dot{V}_r$. End-inspiratory imaging of a tracer gas tends to overestimate the regional ventilation because the conducting airways are filled with the inspired tracer concentration, which increases the apparent rate of rise of the tracer in the alveolar gas by partial volume averaging. For the same reason, end-inspiratory imaging may introduce regional artifacts because of the vary-

ing presence of conducting airways between the inner and outer lung.

Factors affecting the regional distribution of ventilation include local parenchymal compliance, airways resistance and obstruction, regional intrapleural pressure, interdependence effects, tidal volume, gas properties, and respiratory frequency and inspiratory flow rate. Important for the interpretation of pulmonary images, the regional distribution of steady-state, alveolar ventilation is *related to* (but not identical to) the distribution of an inhaled contrast agent or tracer gas during a deep inspiration, nor is it equivalent to the distribution of directly measured changes in regional lung volume. First, the distribution of inspired gas may differ from steady-state breathing for a breath that has different mechanical parameters (flow rate, volume) or gas properties (density, viscosity); second, gas flowing to a lung region without blood flow, for example attributable to a pulmonary embolus, contributes to dead space but not alveolar ventilation. As discussed below, these factors must be considered in formulating questions to address with ventilation imaging as well as for interpreting functional images.

POSTURE AND BREATHING MANUEVERS

Another important consideration for physiologists and imaging scientists is that lung volumes, ventilation, and other mechanical measurements are often made with the subject seated upright, with the most gravitationally dependent regions against the diaphragm. In the upright posture, ventilation in these inferior regions is typically increased relative to superior regions, reflecting variations in regional lung and chest wall mechanics. Physiological insights regarding global ventilation heterogeneity (i.e., the variance of ventilation distribution) have been obtained using indirect measurements in upright subjects, such as single- or multiple-breath nitrogen washouts (62, 66) and computational modeling (15). By contrast, most imaging is performed with patients in the supine or prone position, and thus measures regional ventilation distribution under very different conditions compared with upright measurements. Such differences are important to keep in mind as we review key findings relating imaging to ventilation. Although it is true that many physiological tests may be performed supine to better compare results with imaging (i.e., spirometry), most of human physiology (except for sleeping) is undertaken while upright, arguing for the development of regional imaging methods that can be performed on subjects in the upright position.

Another important consideration is the inhalation and breath-hold maneuvers undertaken when acquiring CT and MRI and how these compare to standard pulmonary function tests. In Table 1, we summarize some of these inhalation and breath-hold approaches (already established in the literature) for the static and dynamic MR and CT imaging techniques discussed in this review.

UNANSWERED QUESTIONS FROM THE PHYSIOLOGIST

Because ventilation is the primary function of the lung, it stands to reason that pulmonary disease is associated with abnormalities in ventilation. However, the lung has considerable reserve capacity, and as such may harbor significant abnormalities not easily detected from clinical symptoms or indices of global lung function. For example in chronic obstructive lung disease (COPD), abnormalities of distal or small airways may not be apparent because of their relatively small contribution to flow measured at the mouth, resulting in minimal alterations in FEV_1 or FVC. Nevertheless, global physiological measurements made at the airway opening have been used to infer ventilation and its heterogeneity throughout the lung. These well-established methods, based on flow, volume, and detection of inert gas wash-in and wash-out profiles, were developed to address mechanistic questions regarding normal and abnormal lung function (18, 25, 67). The critical need for spatial or regional estimates of lung function has motivated the application of imaging methods to these physiological questions.

For patients with chronic diseases such as asthma or COPD, abnormalities of the airways and parenchyma may go undetected by spirometry and the patient themselves because the lung is relatively overengineered for day-to-day living. This chronicity of unresolved inflammation results in progressive worsening of pathology (16). In asthma, some symptoms can be managed with β-agonists, corticosteroids, or leukotriene inhibitors. However, in COPD, deterioration in lung function is usually irreversible, and the thoracic cavity becomes larger as an adaptive response to air trapping, increased compliance, and decreased expiratory flows (20, 23). All of these important physiological changes may be detectable on a regional basis prior to apparent clinical symptomatology and thus less amenable to treatment. Importantly, many therapies for asthma and COPD follow the inhaled route, and the spatial heterogeneity of disease may also result in heterogeneous therapy delivery. Hence regional imaging methods and measurements may be used to help guide therapy (for regional therapy such as

Table 1. *Summary of inhalation and breath-hold approaches*

	Breath Hold	Free Breathing/Gated
CT		
Inspiration/expiration	√	No
Xe CT	√	Gated to controlled or trained breathing
Dual energy Xe CT	Fixed volume inhalation for single breath method	Gated to controlled or trained breathing
Dynamic (4DCT)	No	Tidal breathing
MRI		
Hyperpolarized Xe/He	Fixed volume dose from FRC or RV	Inhalation and exhalation dynamic possible
O_2-enhanced ^1H	No	Tidal breathing
^1H-UTE	Fixed volume inhalation from FRC or RV	No
4D (FD) ^1H	No	Tidal breathing

CT, computed tomography; UTE, ultrashort echo time; FD, Fourier decomposition.

thermoablation or lung reduction strategies) or spatially resolve the effects of therapy. As another example, in syndromes such as acute lung injury, regional abnormalities of ventilation are very common, and mechanical ventilation can accelerate disease progression. Current approaches to ventilator management attempt to restore collapsed or flooded lung regions of ventilation lung while simultaneously avoiding overdistension of already open lung regions, in effect reducing mechanical stresses and ventilation heterogeneity (37, 59). Clearly, there is a need for better regional assessment of lung function in patients with acute and chronic lung disease.

Accordingly, some of the important mechanistic questions for the physiologist interrogating these pathways relate to *1*) regional detection and measurement of structure-function abnormalities prior to symptomatology; *2*) understanding regional pathophysiology and measuring subtle regional responses to therapy; *3*) improved phenotyping or patient stratification based on structural and functional abnormalities; and *4*) utilizing regional characterizations to predict important clinical outcomes such as acute exacerbations, disease progression, and mortality.

SOLUTIONS AND ANSWERS PROVIDED BY IMAGING

The development of functional imaging protocols in pulmonary physiology is resource intensive, and immediate benefits to patients with lung disease are not yet apparent. Thus the question remains: what is the clinical utility of functional lung imaging? The answer is straightforward: in vivo medical imaging, even at relatively low spatial and temporal resolutions, provides a foundation for understanding pulmonary pathophysiology as heterogeneous, regional phenomena (38). Gas phase tracers or contrast agents can be used to estimate gas distribution and even regional ventilation using single breath or multibreath methods. Methods that measure regional oxygen or carbon dioxide concentration or use tracers that exchange with the circulation can be used to estimate important local ventilation/perfusion relationships. Image registration techniques quantify spatial parenchymal deformation and strain, providing a surrogate for ventilation (36) and quantifying local pulmonary mechanical properties. We summarize x-ray CT (with or without the use of inhaled xenon or krypton signal enhancement and using single-energy or dual-energy approaches) and MRI in terms of their corresponding strengths, weaknesses, and availability for research and patient care. In Table 2, we provide a summary of these imaging methods, their spatial and temporal resolution, and typical measurements that can be generated or derived from the images acquired. We think it is also important to acknowledge that there has been limited experience in comparing physiological tests and images in the same person, even with the availability of three-dimensional (3D) volumetric lung measurements derived from CT and MRI. For some examples in Table 2, we provide some of the basic relationships that have been determined between imaging and more established pulmonary function measurements.

Table 2. *Summary of imaging methods*

	Time for Exam	Radiation Dose*	Spatial Resolution	Temporal Resolution	Imaging Measurements
CT					
Inspiration/expiration	5–10 min Total	2–5 mSv for 2-whole lung scans	Up to 0.5 mm isotropic	Up to 0.3 s slice, <5 s whole lung	Specific volume change
Xe CT	approximately 10–20 min Total	High for washin/washout studies-depends on protocol and extent of lung imaged	Up to 0.5 mm isotropic	Up to 0.3 s slice, <5 s whole lung	Specific ventilation
Dual energy Xe CT	5–10 min Total	High for washin/washout studies 1–5 mSv for single breath	Up to 0.5 mm isotropic	Up to 0.3 s slice, <5 s whole lung	Specific ventilation, inhaled gas distribution
4DCT	10–20 min Total	30–40 mSv for low pitch helical study	Up to 0.5 mm isotropic	Up to 0.3 s slice, <5 s whole lung	Specific volume change
MRI					
Hyperpolarized Xe/He	approximately 5–10 min Total	None	2D 3mmx10 mm 3D isotropic 3 mm voxels	15 s acquisition 3D 40 cmx 40 cmx 30 cm every 20–30 s	Inhaled Gas distribution VDV, VDP, PVV
O_2-enhanced ^1H	approximately 30–60 min Total	None	3 mm isotropic voxels		Specific ventilation
UTE ^1H static	approximately 5–10 min Total	None	1 mm voxels	3D 40 cmx 40 cmx 30 cm every 20–30 s	^1H Signal intensity
4D (FD) ^1H	approximately 20–30 min Total	none	3 mm voxels	90 s acquisition	

*mSv, milliSievert WBDE (whole body dose equivalent). Compare with 3–10 mSv for standard dose chest helical CT, 1–2.5 mSv for low-dose helical chest CT, average background radiation exposure of 3–4 mSv/yr.

Multidetector X-Ray Computed Tomography

Since its introduction in the 1970s, CT has provided tremendous insight into the structural and anatomic basis of lung disease that has been supplemented in recent years by its increasing ability to provide functional imaging measurements, including estimates of regional pulmonary ventilation, perfusion, and mechanics. Among the numerous advantages that CT provides include its wide availability and high spatial resolution, with concomitant anatomic and pathologic correlation. Currently available CT scanners are capable of true dynamic volumetric imaging with subsecond temporal resolution, allowing imaging of the entire thorax in less than 3 s, i.e., within a single breathhold even in dyspneic patients. Two major challenges still remain, however, and these are related to lowering the exposure to ionizing radiation by incorporating imaging protocol optimization, and other methods, and translating practical image processing tools into mainstream research and clinical workflows. For example, conventional, 4D and dual energy thoracic CT still results in ~100–500 times the dose of a chest x-ray radiograph (or 1–5 times the annual background radiation).

Tissue contrast in CT stems from the differential attenuation of x-rays by different atomic materials measured in Hounsfield units (HU), which is scaled in an arbitrary and linear fashion with zero defined as the attenuation of x-rays in water and, at the other end of the scale, −1,000 for the attenuation of x-rays in air. The volume averaged signal from the lung parenchyma is linearly related to the proportion of air and tissue; as lung volume increases, the quantity of gas increases while the tissue remains the same and, therefore, overall lung density decreases as the lung expands. Changes in CT density provide accurate measurements of regional and global lung air and tissue volumes as well as an indication of the heterogeneity of lung expansion. To allow quantitation of regional gas movement and mixing, stable radio-dense gaseous xenon (Xe) or krypton (Kr) can be used as tracers or contrast agents (32, 48). Because Xe gas is denser than air, the CT density of an airspace containing Xe increases linearly with Xe concentration (~80 HU maximum density increase with 40% Xe at 80 kV). The rate of Xe wash-in and -out of the parenchyma during steady-state breathing can therefore be estimated from serial CT images on a high-resolution, regional basis and used to quantify regional specific ventilation. This method entails repeat imaging with substantial radiation exposure and the anesthetic properties of Xe limit its concentration in humans (33). Therefore, approaches to reduce the number of images, including single breath methods, and to increase sensitivity and signal-to-noise ratio (SNR), such as dual energy Xe-CT have also been explored. Dual energy Xe-CT uses the differential absorbance of xenon at energies above and below its K_{edge} to generate an image of the contrast agent alone, reducing the noise associated with the density of the lung parenchyma (11). As discussed earlier, the use of an airway tracer gas to measure ventilation may not necessarily correlate directly with either regional CO_2 elimination or O_2 uptake, because both are determined by regional $\dot{V}/\dot{Q}$ ratio rather than $\dot{V}_A$ alone and it assumes that the rate of transfer of the tracer into and out of the alveoli is similar to that of CO_2 elimination. Certainly, this approach is subject to the limitation of the potential differences in gas transport and changes to ventilation distribution of the extremely dense Xe gas, with 40% Xe in air ~50% denser than air alone (14). In this regard, Kr gas is theoretically more suitable because it is 1/3 less dense than Xe and has no anesthetic side effects; however, because it is also less radiodense the contrast enhancement achieved is only 25–30% of that of Xe (13).

Xe is moderately soluble in blood, and its uptake by the circulation is the basis for its use in the measurement of cerebral blood flow (26) and as an inhaled anesthetic (47). This uptake has been used to successfully estimate regional $\dot{V}/\dot{Q}$ ratios from Xe-CT images (43), although translating this technique to clinical use will be challenging because maximizing the signal-to-noise ratio required the use of high Xe concentrations that would be anesthetic in humans. Alternatively, methods for measuring regional pulmonary perfusion with CT from repeat imaging during bolus contrast injection (19) or coregistered SPECT (10) can potentially be used to estimate regional $\dot{V}/\dot{Q}$ ratios.

An alternate approach to estimating regional ventilation with CT is to image the lung at two volumes (ideally end expiration and end inspiration) and then exploit the high-resolution anatomic detail of CT images to measure regional changes in lung volume [specific volume change, sVol = (volume change)/(initial volume)]. sVol is an estimate of regional ventilation only if one assumes that the volume change occurred because of the inflow of fresh gas in to the region. Nonrigid lung registration techniques can be used to map anatomic details, voxel by voxel, from one lung volume to the other (31, 61) and the volume change measured from the calculated deformation of each voxel (3) or, alternatively, from the density change of the corresponding mapped lung regions (29, 31). Compared with the Xe-CT approach, this so-called 4DCT ventilation estimate cannot distinguish actual inflow of fresh gas (ventilation) from redistribution of alveolar or dead space gas (pendelluft), but it does provide a reasonable surrogate for regional ventilation that has been validated in healthy lungs (29, 61). Evolving techniques for gated imaging or retrospective reconstruction of the whole lung during uncontrolled or "free" tidal breathing make this technique increasingly attractive for use in patients (8, 31). As shown in Fig. 1, this approach also provides novel insights into regional lung mechanical behavior on a finer spatial scale than previously possible (36). A direct comparison between 4DCT and ^{3}He-MRI estimates of pulmonary ventilation is provided in Fig. 2. It is important to note, however, that with all methods that involve multiple image acquisitions and the requirement for image registration, there is a potential source of error because of the elastic nature of the lung. More technically demanding, nonrigid registration methods are required in these cases, although there is still the potential for error in the generation of ventilation maps. We also must acknowledge that in such cases where static or dynamic imaging is suggestive of ventilation abnormalities, in most cases there has been no comparison to ground truth (histopathology) so the exact etiology of such abnormalities is not known. Therefore, for example in Fig. 2, there is no way to normalize color scales for 4DCT and ^{3}He-MRI because ground truth is not known. By way of example, we note that the differences in relative intensities of gas in the trachea (4DCT trachea is devoid of gas compared with ^{3}He-MRI

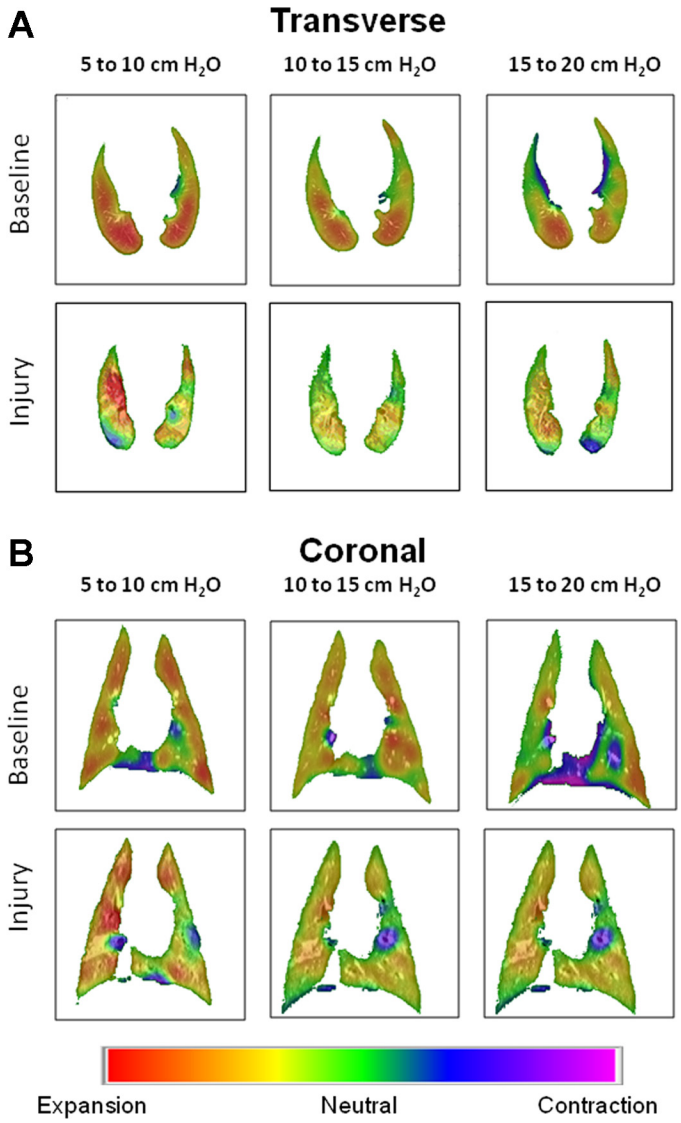

Fig. 1. Regional parenchymal deformation maps obtained using CT image registration in transverse (*A*) and coronal (*B*) sections for a supine dog at baseline and following acute lung injury (ALI) induced by the infusion of oleic acid into the pulmonary artery. Computed tomography (CT) images were obtained during constant breath holds at 5, 10, 15, and 20 cmH_2O transrespiratory pressure. Registrations were performed for 3 different inflation pressures pairs: 5–10 cmH_2O, 10–15 cmH_2O, and 15–20 cmH_2O. Volume changes are color coded such that yellow, orange, and red correspond to expansion; blue and purple to contraction; and green to no change in volume. Note that during baseline conditions, the lungs exhibited fairly uniform expansion throughout the transverse section for lower inflation pressures, although the registration algorithm does predict small regions of compression occurring near the mediastinum. For more moderate inflation pressures, expansion occurs preferentially in more dependent regions. Following ALI, expansion fields are more heterogeneous at all inflation pressures, with regions of relative compression interspersed throughout the transverse sections. [Figure modified from Kaczka et al. (36) with permission.]

that is gas filled) might reflect the differences in the breathing maneuvers used for image acquisition (see Table 1).

Magnetic Resonance Imaging

In contrast to CT-based methods, the use of MRI for assessment of pulmonary function is relatively recent. Except in very limited situations, pulmonary MRI is still considered a research tool. The reasons for this relate directly to the structure and function of the respiratory system and the physics of MRI, both of which represent fundamental challenges that have limited the utility of conventional ^{1}H-MRI for pulmonary disease. Conventional MRI tissue contrast stems from the perturbation of water- and fat-bound hydrogen atoms [otherwise known as protons (^{1}H)] using a burst of radiofrequency energy. The MRI signal derives from the tiny net fraction of protons that are aligned with the magnetic field of the scanner, and after application of radiofrequency radiation, these undergo realignment that is detected and converted into the image. The lung has very low tissue and proton density, and therefore pulmonary MRI, even when optimized for the lung, results in images (39, 42) with lung regions mainly devoid of contrast, tissue, and morphological information (Fig. 3). Compounding this, the different magnetic environments related to the tightly spaced air and tissue compartments result in so-called magnetic susceptibility artifacts that accelerate signal decay, i.e., less signal is available for imaging in a given time window compared with organs with a higher proton density such as, for example, the liver or the muscles. For these reasons, the development of conventional pulmonary MRI has been mainly overlooked as a clinical application, although its diagnostic potential was recognized nearly three decades ago (54). Pulmonary applications

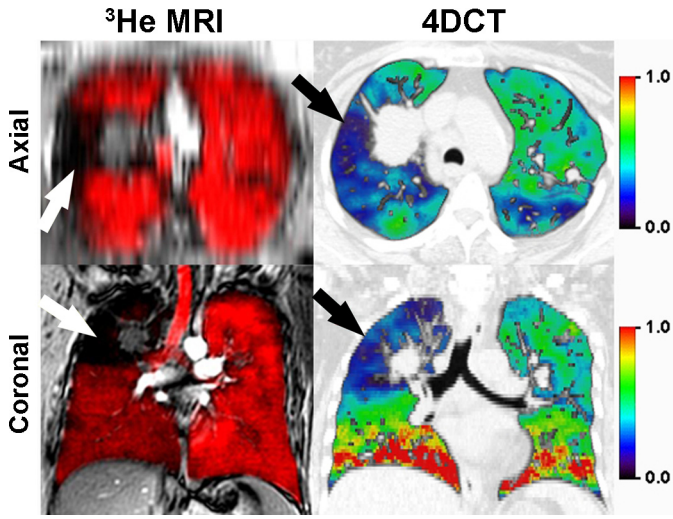

Fig. 2. Hyperpolarized ^{3}He-MRI coregistered with ^{1}H-MRI as well as 4DCT acquired within 7 days in a single non-small cell lung cancer patient. *Top*: axial reconstructions; *bottom*: coronal slices. Magnetic resonance imaging (MRI) was obtained in the coronal plane during inspiration breath hold, after inhalation of a 1 liter gas mixture of hyperpolarized ^{3}He and ultra-high purity N_2 gas from functional residual capacity. ^{1}H-MRI preceded ^{3}He-MRI by ~5 min and the ^{1}H- and ^{3}He-MRI slices were rigidly coregistered using the carina for fiducial landmarks. To generate the 4DCT ventilation maps, first, thoracic CT images were acquired during a single tidal breathing maneuver (120 kV, 60–120 mA, rotation time of 0.5 s, 360° reconstruction, pitch <0.1). CT images were reconstructed at 10 different respiratory phases and tagged as a percent of full inspiration, with in plane resolution of 1.0 mm. Deformable image registration methods were used to generate a ventilation map. Coregistered ^{1}H (gray scale)- and ^{3}He-MRI gas distribution images show gas in red, and focal ventilation defects are clearly shown where the ^{1}H thoracic cavity is exposed (in black) in the absence of gas. 4DCT ventilation maps are color-coded differently such that red, orange, and yellow correspond to regions of greater ventilation; and blue, purple, and black correspond to regions of lower or no ventilation with green representing average values. Note that there is a qualitative regional correspondence between 4DCT regions of decreased ventilation and MRI regions of ventilation defects.

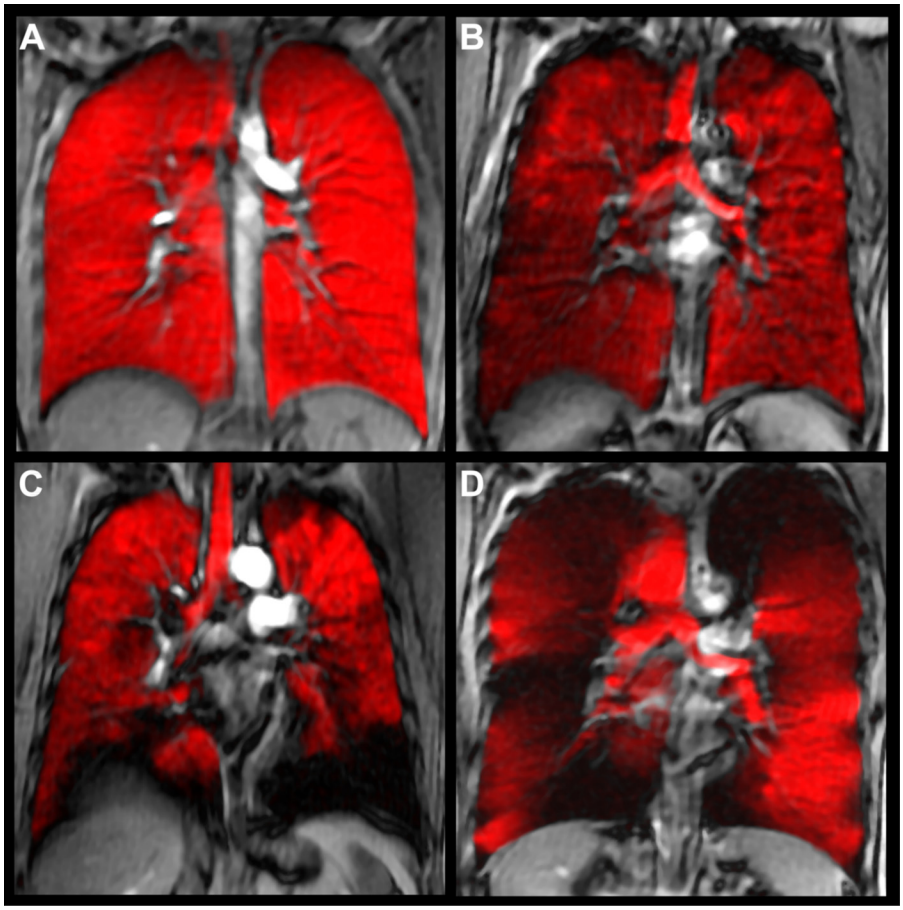

Fig. 3. Hyperpolarized ^{3}He-MRI of gas distribution (in red) coregistered to ^{1}H-MRI of thoracic cavity (gray scale) of a healthy young never-smoker (*A*), older never-smoker (*B*), asthma (*C*), and COPD (*D*). MRI was obtained in the coronal plane during inspiration breath hold, after inhalation of a 1 liter gas mixture of hyperpolarized ^{3}He and ultra-high purity N_2 gas from functional residual capacity. ^{1}H-MRI preceded ^{3}He-MRI by ~5 min and the ^{1}H- and ^{3}He-MRI slices were coregistered using rigid registration methods using the carina for fiducial landmarks. Coregistered ^{1}H (gray scale)- and ^{3}He-MRI gas distribution images show gas in red, and focal ventilation defects are clearly shown where the ^{1}H thoracic cavity is exposed (in black) in the absence of gas. Note the absence of gas distribution abnormalities in *A* for the healthy young never-smokers, but there are qualitative differences for the elderly never-smoker and much more obvious abnormalities in asthma (*C*) and COPD (*D*). Some qualitative differences can also be observed in the gas distribution obvious in the trachea, although for all subjects, the breath-hold maneuver was the same.

of ^{1}H-MRI have been further developed (4, 5) with renewed interest in the potential of pulmonary MRI stimulated by novel pulmonary functional MRI techniques using noble gas contrast agents (28) as well as oxygen-enhanced (53) and Fourier-decomposition ^{1}H-MRI (6, 7).

Noble gas MRI, first described for ^{129}Xe (1), provides a way to visualize in relatively high spatial resolution the distribution of inhaled gas. In particular, so-called static ventilation imaging provides a map of gas distribution, with imaging typically taking place with the subject in breath hold after inhalation of a discrete volume of magnetized (or hyperpolarized) helium or xenon gas. As shown in Fig. 3, the inhaled gas provides a way to estimate gas distribution after a single inhalation in a variety of subjects. In healthy young adults, a single inhalation and breath hold of hyperpolarized ^{3}He gas results in homogeneous signal, suggesting that all areas of the lung are participating equally in gas distribution (Fig. 3*A*). In contrast, characteristic volumetric focal defects are observed in COPD and asthma and even in otherwise healthy elderly never-smokers (57, 58) as regions that do not appear to contain gas signal (Fig. 3, *B-D*). These are thought to correspond to areas of the lung that do not participate in ventilation or perhaps are poorly ventilated during steady state. Following a single inhalation from FRC and breath hold of tracer gas, focal ^{3}He or ^{129}Xe gas distribution abnormalities (Fig. 4) can be directly quantified. Historically, such abnormalities were qualitatively evaluated as mild, moderate, or severe (2, 65) and then as the field progressed, ventilation defects were counted or scored based on a cluster of voxels appearing to reflect gas intensities at or below the background noise. Manual segmentation of gas distribution abnormalities was also undertaken to generate the absolute volume of the focal defects as the ventilation defect volume (VDV) (58), the normalized ventilation defect percent (VDP) (50, 51), and the percent ventilation volume (PVV) (70), all of which have excellent reproducibility (50). It is important to note, however, that all these functional measurements of the parenchyma depend on gas flow or diffusion through the airways, providing an indirect measurement of airway patency and function (44). Unfortunately, the exact etiology of such gas distribution abnormalities is not known, making it difficult if not impossible to understand if such defects are attributable to airway closure and/or narrowing or perhaps bullous disease (in COPD). Because such defects do not appear to be random but appear regionally fixed and temporally persistent in individual subjects with COPD and asthma, this suggests structural abnormalities such as airway narrowing or closure that is not intermittent. Another consideration is that defects likely reflect time constants for filling that are longer than the relatively short breath-hold static snapshot that is typically acquired. In other words, such images are acquired as a static breath-hold snapshot within the time course of a typical 10- to 15-s scan (52), so the relationship between these functional abnormalities to structural abnormalities and to ventilation (at equilibrium) is not completely clear. What is clear, however, are the numerous advantages of single breath-hold imaging in terms of time, expense, simplicity, patient comfort, and compliance and all of

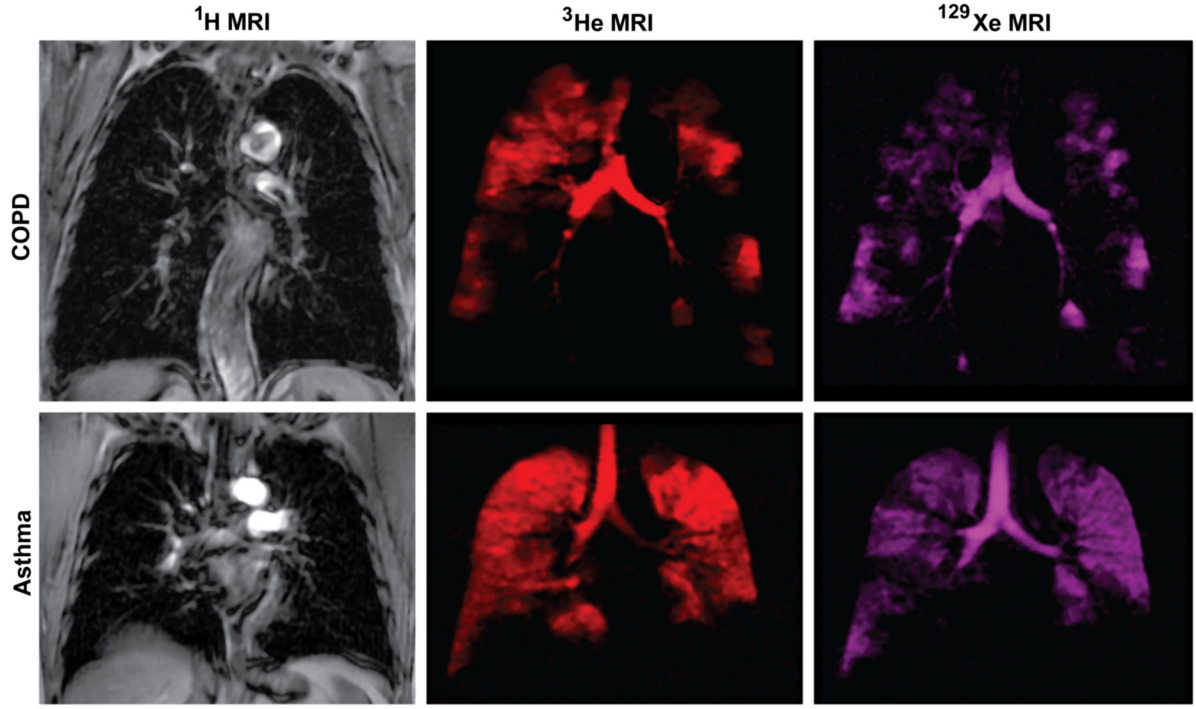

Fig. 4. Conventional ^{1}H-, hyperpolarized ^{3}He- and ^{129}Xe-MRI of a single subject each with COPD and asthma. ^{1}H-MRI of the thoracic cavity (gray scale) was obtained in the coronal plane during inspiration breath hold, after inhalation of 1 liter of ultra-high purity N_2 gas from functional residual capacity (FRC). Within 3 min, the same subject inhaled a 1 liter mixture of hyperpolarized ^{3}He gas mixed with N_2 gas from FRC for static ventilation imaging of ^{3}He gas distribution (shown in red) acquired in a 15 s breath hold. Approximately 3 min later, the subject inhaled a 1 liter mixture of hyperpolarized ^{129}Xe gas mixed with ^{4}He from FRC for static ventilation imaging of ^{129}Xe gas distribution (shown in purple) acquired in a 15 s breath hold. Note the qualitative differences in gas distribution abnormalities that are obvious between ^{129}Xe- and ^{3}He-MRI for both subjects. It is also important to note that the exact etiology of such gas distribution abnormalities has not yet been established. Such differences between ^{3}He- and ^{129}Xe-MRI gas distribution may be attributable to differences in the gas properties such as diffusion, viscosity, or perhaps tissue solubility.

these issues have implications for clinical translation. To address this issue, in Fig. 2 we show a recent direct comparison of a static breath hold ^{3}He-MRI with dynamic 4DCT imaging—both of which can be used to estimate surrogates of ventilation. As shown, there is excellent spatial or regional correlation between gas distribution abnormalities shown using both methods, suggesting that ^{3}He-MRI ventilation defects may indeed be related to airway constriction that also results in 4DCT gas distribution defects that can be generated over a tidal breathing cycle.

Beyond static ventilation imaging with hyperpolarized ^{3}He, an elegant dynamic approach was recently described whereby a single breath hold of ^{3}He gas was employed and the relationship was determined between well-established pneumatograph and ^{3}He-MRI measurements of inert gas washout (22). Pertinent to this review, the novelty of this study directly relates to the use of imaging and pneumotach measurements to calculate TLC and this allows for a better and regional understanding of inert gas washout measurements. The imaging and physiological measurements were in good agreement, showing the predicted regional differences in ventilation as evidenced by differences in residual ^{3}He gas present in the lung after multiple breaths of fresh air. The same team took advantage of time-delayed or time-resolved imaging to directly visualize delayed ^{3}He gas distribution in COPD into regions of the lung that they suggested was due to collateral ventilation (49), providing an important regional description of this critical physiological mechanism.

Finally, we end this discussion of MRI measurements of ventilation and surrogates of ventilation by returning to more conventional ^{1}H-MRI without the use of polarized tracer gases. As already mentioned, lung tissue (parenchyma) MRI can be performed with very short echo times (otherwise known as ultrashort echo time MRI or UTE), thereby minimizing artifacts related to the air-tissue interfaces in the lung (27). In this way, and with subjects in breath hold, images can be acquired to identify regions of low proton intensity that are mainly devoid of tissue (tissue destruction related to bullae/emphysema) (56) or regions of higher proton density that may be related to fluid infiltrates or edema (40, 45, 46, 69). In contrast to this structural information, functional oxygen-enhanced ^{1}H-MRI can also be employed that relies on the innate contrast provided by air or oxygen and the fact that it is weakly paramagnetic, decreasing the longitudinal relaxation time (T1) of the lung parenchyma (35, 55, 64). Accordingly, the change in O_2 concentration in lung tissues is reflected by a local change in T1, and this strictly depends on the rate of change of alveolar O_2 concentration—itself a function of the regional specific ventilation. Oxygen-enhanced ^{1}H-MR images are typically acquired over a series of breathing maneuvers as a pair of images—one set of images acquired with the subject required to inhale oxygen from a mask at concentrations higher than air (typically 100%) and another set of images acquired with the subject inhaling air (21% oxygen). The recent application of this method to describe the vertical distribution of regional ventilation in human subjects (64) provides a good

example of fruitful collaborations between physiologists and imaging scientists to address fundamental questions in pulmonary medicine. In a different application that does not involve oxygen enhancement, tidal breathing of room air can be estimated using dynamic ultra-short echo time ^{1}H-MRI, using the ^{1}H signal intensity of the lung tissue in each voxel that changes as the lung expands and contracts when air moves in and out of the lung. Ingeniously, the Fourier decomposition (FD) of the ^{1}H signal intensity fluctuations that occur during normal tidal breathing of room air can be used to dissect the ventilation (air in and out component of the sinusoidal ^{1}H signal intensity time curve) and the perfusion (blood in and out component of the sinusoidal ^{1}H signal intensity time curve) signals (7). With appropriate registration of the inspiratory and expiratory images, ^{1}H ventilation and perfusion maps can be generated (6). The strength of this approach is the use of conventional scanning equipment and pulse sequences, thus translating the power of functional MRI to any scanner or patient, without the need for magnetized contrast agents or other specialized equipment. Limitations or drawbacks of dynamic or FD MRI for the generation of ventilation images relate to the need for complex image registration algorithms and excellent reproducibility between tidal breaths to ensure adequate image registration.

FUTURE RESEARCH DIRECTIONS AND CHALLENGES FOR THE FUTURE

A variety of CT- and MRI-based methods may now be used for the evaluation of regional lung function, including ventilation. To move such imaging techniques into mainstream scientific research and clinical medicine, tight integration of physiology and imaging science as interdisciplinary fields will be required. Early detection of regional structure-function abnormalities using functional imaging will allow for the testing and development of therapies based on appropriate physiological and anatomic endpoints. Understanding regional pathophysiology and its response to treatment requires accurate and reproducible imaging protocols that are codeveloped by physicists and physiologists with appreciation of the subtle diagnostic information provided by such measurements. Patient phenotyping requires both clinical and scientific awareness of lung disease and the complementary relationship between clinical findings and imaging data. Ultimately functional lung imaging must be evaluated as important and reliable predictors of clinical outcomes, such as acute exacerbations, progressive functional deterioration, and mortality.

ACKNOWLEDGMENTS

We thank our research teams for continued support of this research.

FUNDING

G. Parraga gratefully acknowledges support from the Canadian Institutes of Health Research (CIHR) Operating Grants MOP #97748, MOP #106437, Team Grant FRN #97687, and a CIHR New Investigator award. D. W. Kaczka acknowledges support from National Institutes of Health Grant HL089227.

DISCLOSURES

G. Parraga paid $100,000 annually (2009–2011) for the use of an onsite hyperpolarized ^{3}He gas polarizer [Helispin, General Electric Health Care (GEHC), Durham, NC] and $60,000 for the use of the XeBox-E10 (Xemed LLC, Durham, NH) system for the period September 6–29, 2011. A. A. Bankier receives up to 10.000 USD consultant honorariums from Spiration (Olympus Medical), as well as authorship honoraria from Elsevier publishers.

AUTHOR CONTRIBUTIONS

Author contributions: B.A.S., D.W.K., A.A.B., and G.P. prepared figures; B.A.S., D.W.K., A.A.B., and G.P. drafted manuscript; B.A.S., D.W.K., A.A.B., and G.P. edited and revised manuscript; B.A.S., D.W.K., A.A.B., and G.P. approved final version of manuscript.

REFERENCES

1. **Albert MS, Cates GD, Driehuys B, Happer W, Saam B, Springer CS Jr, Wishnia A.** Biological magnetic resonance imaging using laser-polarized 129Xe. *Nature* 370: 199–201, 1994.
2. **Altes TA, Powers PL, Knight-Scott J, Rakes G, Platts-Mills TA, de Lange EE, Alford BA, Mugler JP III, Brookeman JR.** Hyperpolarized 3He MR lung ventilation imaging in asthmatics: preliminary findings. *J Magn Reson Imaging* 13: 378–384, 2001.
3. **Amelon R, Cao K, Ding K, Christensen GE, Reinhardt JM, Raghavan ML.** Three-dimensional characterization of regional lung deformation. *J Biomech* 44: 2489–2495, 2011.
4. **Bankier AA, Mai VM, Zhang M, Edelman RR, Chen Q.** In-vivo MR imaging of gravity dependent intensity gradients in human lungs. *Proceedings of the 8th Annual Meeting of ISMRM*. Denver, 2000.
5. **Bankier AA, Storey P, Mai VM, Edelman RR, Chen Q.** Gravity-dependent signal gradients on MR images of the lung in supine and prone positions: a comparison with isogravitational signal variability. *J Magn Reson Imaging* 23: 115–122, 2006.
6. **Bauman G, Lutzen U, Ullrich M, Gaass T, Dinkel J, Elke G, Meybohm P, Frerichs I, Hoffmann B, Borggrefe J, Knuth HC, Schupp J, Prum H, Eichinger M, Puderbach M, Biederer J, Hintze C.** Pulmonary functional imaging: qualitative comparison of Fourier decomposition MR imaging with SPECT/CT in porcine lung. *Radiology* 260: 551–559, 2011.
7. **Bauman G, Puderbach M, Deimling M, Jellus V, Chefd'hotel C, Dinkel J, Hintze C, Kauczor HU, Schad LR.** Non-contrast-enhanced perfusion and ventilation assessment of the human lung by means of fourier decomposition in proton MRI. *Magn Reson Med* 62: 656–664, 2009.
8. **Biederer J, Hintze C, Fabel M, Dinkel J.** Magnetic resonance imaging and computed tomography of respiratory mechanics. *J Magn Reson Imaging* 32: 1388–1397, 2010.
9. **Blatter DD, Bahr AL, Parker DL, Robison RO, Kimball JA, Perry DM, Horn S.** Cervical carotid MR angiography with multiple overlapping thin-slab acquisition: comparison with conventional angiography. *Am J Roentgenol Radium Ther* 161: 1269–1277, 1993.
10. **Castillo R, Castillo E, McCurdy M, Gomez DR, Block AM, Bergsma D, Joy S, Guerrero T.** Spatial correspondence of 4D CT ventilation and SPECT pulmonary perfusion defects in patients with malignant airway stenosis. *Phys Med Biol* 57: 1855–1871, 2012.
11. **Chae EJ, Seo JB, Goo HW, Kim N, Song KS, Lee SD, Hong SJ, Krauss B.** Xenon ventilation CT with a dual-energy technique of dual-source CT: initial experience. *Radiology* 248: 615–624, 2008.
12. **Chen DL, Schuster DP.** Imaging pulmonary inflammation with positron emission tomography: a biomarker for drug development. *Mol Pharm* 3: 488–495, 2006.
13. **Chon D, Beck KC, Simon BA, Shikata H, Saba OI, Hoffman EA.** Effect of low-xenon and krypton supplementation on signal/noise of regional CT-based ventilation measurements. *J Appl Physiol* 102: 1535–1544, 2007.
14. **Chon D, Simon BA, Beck KC, Shikata H, Saba OI, Won C, Hoffman EA.** Differences in regional wash-in and wash-out time constants for xenon-CT ventilation studies. *Respir Physiol Neurobiol* 148: 65–83, 2005.
15. **Colletti AA, Amini R, Kaczka DW.** Simulating ventilation distribution in heterogenous lung injury using a binary tree data structure. *Comput Biol Med* 41: 936–945, 2011.
16. **Cosio MG, Saetta M, Agusti A.** Immunologic aspects of chronic obstructive pulmonary disease. *N Engl J Med* 360: 2445–2454, 2009.
17. **Coyne TJ, Wallace MC.** Surgical referral for carotid artery stenosis—the influence of NASCET. North American Symptomatic Carotid Endarterectomy Trial. *Can J Neurol Sci* 21: 129–132, 1994.
18. **Crawford AB, Makowska M, Paiva M, Engel LA.** Convection- and diffusion-dependent ventilation maldistribution in normal subjects. *J Appl Physiol* 59: 838–846, 1985.

19. **Dakin JH, Evans TW, Hansell DM, Hoffman EA.** Regional pulmonary blood flow in humans and dogs by 4D computed tomography. *Acad Radiol* 15: 844–852, 2008.
20. **Decramer M, Janssens W, Miravitlles M.** Chronic obstructive pulmonary disease. *Lancet* 379: 1341–1351, 2012.
21. **Deninger AJ, Mansson S, Petersson JS, Pettersson G, Magnusson P, Svensson J, Fridlund B, Hansson G, Erjefeldt I, Wollmer P, Golman K.** Quantitative measurement of regional lung ventilation using 3He MRI. *Magn Reson Med* 48: 223–232, 2002.
22. **Deppe MH, Parra-Robles J, Ajraoui S, Wild JM.** Combined measurement of pulmonary inert gas washout and regional ventilation heterogeneity by MR of a single dose of hyperpolarized 3He. *Magn Reson Med* 65: 1075–1083, 2011.
23. **Doherty DE.** The pathophysiology of airway dysfunction. *Am J Med* 117, Suppl 12A: 11S–23S, 2004.
24. **Dolovich MB, Schuster DP.** Positron emission tomography and computed tomography versus positron emission tomography computed tomography: tools for imaging the lung. *Proc Am Thorac Soc* 4: 328–333, 2007.
25. **Downie SR, Salome CM, Verbanck S, Thompson B, Berend N, King GG.** Ventilation heterogeneity is a major determinant of airway hyperresponsiveness in asthma, independent of airway inflammation. *Thorax* 62: 684–689, 2007.
26. **Drayer BP, Wolfson SK, Reinmuth OM, Dujovny M, Boehnke M, Cook EE.** Xenon enhanced CT for analysis of cerebral integrity, perfusion, and blood flow. *Stroke* 9: 123–130, 1978.
27. **Edelman RR, Hatabu H, Tadamura E, Li W, Prasad PV.** Noninvasive assessment of regional ventilation in the human lung using oxygen-enhanced magnetic resonance imaging. *Nat Med* 2: 1236–1239, 1996.
28. **Fain S, Schiebler ML, McCormack DG, Parraga G.** Imaging of lung function using hyperpolarized helium-3 magnetic resonance imaging: Review of current and emerging translational methods and applications. *J Magn Reson Imaging* 32: 1398–1408, 2010.
29. **Fuld MK, Easley RB, Saba OI, Chon D, Reinhardt JM, Hoffman EA, Simon BA.** CT-measured regional specific volume change reflects regional ventilation in supine sheep. *J Appl Physiol* 104: 1177–1184, 2008.
30. **Gasecki AP, Eliasziw M, Ferguson GG, Hachinski V, Barnett HJ.** Long-term prognosis and effect of endarterectomy in patients with symptomatic severe carotid stenosis and contralateral carotid stenosis or occlusion: results from NASCET. North American Symptomatic Carotid Endarterectomy Trial (NASCET) Group. *J Neurosurg* 83: 778–782, 1995.
31. **Guerrero T, Sanders K, Castillo E, Zhang Y, Bidaut L, Pan T, Komaki R.** Dynamic ventilation imaging from four-dimensional computed tomography. *Phys Med Biol* 51: 777–791, 2006.
32. **Gur D, Drayer BP, Borovetz HS, Griffith BP, Hardesty RL, Wolfson SK.** Dynamic computed tomography of the lung: regional ventilation measurements. *J Comput Assist Tomogr* 3: 749–753, 1979.
33. **Gur D, Shabason L, Borovetz HS, Herbert DL, Reece GJ, Kennedy WH, Serago C.** Regional pulmonary ventilation measurements by xenon enhanced dynamic computed tomography: an update. *J Comput Assist Tomogr* 5: 678–683, 1981.
34. **Harris RS, Schuster DP.** Visualizing lung function with positron emission tomography. *J Appl Physiol* 102: 448–458, 2007.
35. **Jakob PM, Wang T, Schultz G, Hebestreit H, Hebestreit A, Hahn D.** Assessment of human pulmonary function using oxygen-enhanced T(1) imaging in patients with cystic fibrosis. *Magn Reson Med* 51: 1009–1016, 2004.
36. **Kaczka DW, Cao K, Christensen GE, Bates JH, Simon BA.** Analysis of regional mechanics in canine lung injury using forced oscillations and 3D image registration. *Ann Biomed Eng* 39: 1112–1124, 2011.
37. **Kaczka DW, Hager DN, Hawley ML, Simon BA.** Quantifying mechanical heterogeneity in canine acute lung injury: impact of mean airway pressure. *Anesthesiology* 103: 306–317, 2005.
38. **Kaczka DW, Lutchen KR, Hantos Z.** Emergent behavior of regional heterogeneity in the lung and its effects on respiratory impedance. *J Appl Physiol* 110: 1473–1481, 2011.
39. **Kauczor HU, Ley S.** Thoracic magnetic resonance imaging 1985 to 2010. *J Thorac Imaging* 25: 34–38, 2010.
40. **Kauczor HU, Ley-Zaporozhan J, Ley S.** Imaging of pulmonary pathologies: focus on magnetic resonance imaging. *Proc Am Thorac Soc* 6: 458–463, 2009.
41. **Kety SS.** The theory and applications of the exchange of inert gas at the lungs and tissues. *Pharmacol Rev* 3: 1–41, 1951.
42. **Kirby M, Owrangi A, Wong J, Costella S, Choy S, McCormack DG, Parraga G.** Pulmonary magnetic resonance imaging of obstructive airways disease. *Minerva Pnemologica* 50: 17–19, 2011.
43. **Kreck TC, Krueger MA, Altemeier WA, Sinclair SE, Robertson HT, Shade ED, Hildebrandt J, Lamm WJ, Frazer DA, Polissar NL, Hlastala MP.** Determination of regional ventilation and perfusion in the lung using xenon and computed tomography. *J Appl Physiol* 91: 1741–1749, 2001.
44. **Leary D, Bhatawadekar SA, Parraga G, Maksym GN.** Modeling stochastic and spatial heterogeneity in a human airway tree to determine variation in respiratory system resistance. *J Appl Physiol* 112: 167–175, 2012.
45. **Ley-Zaporozhan J, Ley S, Sommerburg O, Komm N, Muller FM, Schenk JP.** Clinical application of MRI in children for the assessment of pulmonary diseases. *Rofo Fortschr Geb Rontgenstr Neuen Bildgeb Verfahr* 181: 419–432, 2009.
46. **Ley-Zaporozhan J, Puderbach M, Kauczor HU.** MR for the evaluation of obstructive pulmonary disease. *Magn Reson Imaging Clin N Am* 16: 291–308, ix, 2008.
47. **Lynch C III, Baum J, Tenbrinck R.** Xenon anesthesia. *Anesthesiology* 92: 865–868, 2000.
48. **Marcucci C, Nyhan D, Simon BA.** Distribution of pulmonary ventilation using Xe-enhanced computed tomography in prone and supine dogs. *J Appl Physiol* 90: 421–430, 2001.
49. **Marshall H, Deppe MH, Parra-Robles J, Hillis S, Billings CG, Rajaram S, Swift A, Miller SR, Watson JH, Wolber J, Lipson DA, Lawson R, Wild JM.** Direct visualisation of collateral ventilation in COPD with hyperpolarised gas MRI. *Thorax*; in press.
50. **Mathew L, Evans A, Ouriadov A, Etemad-Rezai R, Fogel R, Santyr G, McCormack DG, Parraga G.** Hyperpolarized 3He magnetic resonance imaging of chronic obstructive pulmonary disease: reproducibility at 3.0 tesla. *Acad Radiol* 15: 1298–1311, 2008.
51. **Mathew L, Gaede S, Wheatley A, Etemad-Rezai R, Rodrigues GB, Parraga G.** Detection of longitudinal lung structural and functional changes after diagnosis of radiation-induced lung injury using hyperpolarized 3He magnetic resonance imaging. *Med Phys* 37: 22–31, 2010.
52. **Mathew L, Kirby M, Etemad-Rezai R, Wheatley A, McCormack DG, Parraga G.** Hyperpolarized (3)He magnetic resonance imaging: preliminary evaluation of phenotyping potential in chronic obstructive pulmonary disease. *Eur J Radiol* 79: 140–146, 2011.
53. **Matsuoka S, Hunsaker AR, Gill RR, Jacobson FL, Ohno Y, Patz S, Hatabu H.** Functional MR imaging of the lung. *Magn Reson Imaging Clin N Am* 16: 275–289, ix, 2008.
54. **Mayo JR, MacKay A, Muller NL.** MR imaging of the lungs: value of short TE spin-echo pulse sequences. *Am J Roentgenol Radium Ther* 159: 951–956, 1992.
55. **Ohno Y, Hatabu H.** Basics concepts and clinical applications of oxygen-enhanced MR imaging. *Eur J Radiol* 64: 320–328, 2007.
56. **Ohno Y, Koyama H, Nogami M, Takenaka D, Matsumoto S, Obara M, Sugimura K.** Dynamic oxygen-enhanced MRI versus quantitative CT: pulmonary functional loss assessment and clinical stage classification of smoking-related COPD. *Am J Roentgenol Radium Ther* 190: W93-W99, 2008.
57. **Parraga G, Mathew L, Etemad-Rezai R, McCormack DG, Santyr GE.** Hyperpolarized 3He magnetic resonance imaging of ventilation defects in healthy elderly volunteers: initial findings at 3.0 Tesla. *Acad Radiol* 15: 776–785, 2008.
58. **Parraga G, Ouriadov A, Evans A, McKay S, Lam WW, Fenster A, Etemad-Rezai R, McCormack D, Santyr G.** Hyperpolarized 3He ventilation defects and apparent diffusion coefficients in chronic obstructive pulmonary disease: preliminary results at 3.0 Tesla. *Invest Radiol* 42: 384–391, 2007.
59. **Pelosi P, Rocco PR.** Ventilator-induced lung injury in healthy and diseased lungs: better to prevent than cure! *Anesthesiology* 115: 923–925, 2011.
60. **Petersson J, Sanchez-Crespo A, Larsson SA, Mure M.** Physiological imaging of the lung: single-photon-emission computed tomography (SPECT). *J Appl Physiol* 102: 468–476, 2007.
61. **Reinhardt JM, Ding K, Cao K, Christensen GE, Hoffman EA, Bodas SV.** Registration-based estimates of local lung tissue expansion compared to xenon CT measures of specific ventilation. *Med Image Anal* 12: 752–763, 2008.

62. **Roca J, Wagner PD.** Contribution of multiple inert gas elimination technique to pulmonary medicine. 1 Principles and information content of the multiple inert gas elimination technique. *Thorax* 49: 815–824, 1994.
63. **Rotstein AH, Gibson RN, King PM.** Direct B-mode NASCET-style stenosis measurement and Doppler ultrasound as parameters for assessment of internal carotid artery stenosis. *Australas Radiol* 46: 52–56, 2002.
64. **Sa RC, Cronin MV, Henderson AC, Holverda S, Theilmann RJ, Arai TJ, Dubowitz DJ, Hopkins SR, Buxton RB, Prisk GK.** Vertical distribution of specific ventilation in normal supine humans measured by oxygen-enhanced proton. *MRI J Appl Physiol* 109: 1950–1959, 2010.
65. **Samee S, Altes T, Powers P, de Lange EE, Knight-Scott J, Rakes G, Mugler JP III, Ciambotti JM, Alford BA, Brookeman JR, Platts-Mills TA.** Imaging the lungs in asthmatic patients by using hyperpolarized helium-3 magnetic resonance: assessment of response to methacholine and exercise challenge. *J Allergy Clin Immunol* 111: 1205–1211, 2003.
66. **Verbanck S, Paiva M, Schuermans D, Hanon S, Vincken W, Van MA.** Relationships between the lung clearance index and conductive and acinar ventilation heterogeneity. *J Appl Physiol* 112: 782–790, 2012.
67. **Verbanck S, Schuermans D, Meysman M, Paiva M, Vincken W.** Noninvasive assessment of airway alterations in smokers: the small airways revisited. *Am J Respir Crit Care Med* 170: 414–419, 2004.
68. **West JB.** *Respiratory Physiology: The Essentials*. Philadelphia: Lippincott Williams & Wilkins, 2008.
69. **Wielputz M, Kauczor HU.** MRI of the lung: state of the art. *Diagn Interv Radiol*; in press.
70. **Woodhouse N, Wild JM, Paley MN, Fichele S, Said Z, Swift AJ, van Beek EJ.** Combined helium-3/proton magnetic resonance imaging measurement of ventilated lung volumes in smokers compared to never-smokers. *J Magn Reson Imaging* 21: 365–369, 2005.